A Photoaddressable Liquid Crystalline Phase Transition in Graphene Oxide Nanocomposites

Crespo, Maria; Santagiuliana, Giovanni; Picot, Olivier; Portale, Giuseppe; Bilotti, Emiliano; Gautrot, Julien E.

Published in:
Advanced Functional Materials

DOI:
10.1002/adfm.201900738

Publication date:
2019

ADVANCED FUNCTIONAL MATERIALS
www.afm-journal.de

A Photoaddressable Liquid Crystalline Phase Transition in Graphene Oxide Nanocomposites

Maria Crespo, Giovanni Santagiuliana, Olivier Picot, Giuseppe Portale, Emiliano Bilotti,* and Julien E. Gautrot**

The multifunctionality of graphene has the potential to unlock important developments in nanocomposite science. However, the manipulation of graphene without interfering with its unique properties and while controlling its spatial organization remains challenging. Here, the formation of a photoaddressable liquid crystalline (LC) solution through the stabilization of graphene oxide (GO) with photocleavable brushes is described. The LC behavior leads to the thermodynamic entrapment of GO into low aspect ratio domains that fail to display the properties typically predicted for graphene nanocomposites. The morphology and structural and electronic performance of these nanocomposites are regenerated through the brush cleavage, which controls the phase transition of the LC phase. These results show that kinetic control of graphene assembly can be an attractive tool toward the dynamic regulation of processable sol states and structured percolated networks for rational composite manufacturing.

1. Introduction

Graphene's exceptional physicochemical characteristics have led to its uptake for a host of composite applications.[1,2] The intrinsic performance of these materials is mainly dependent on the number of layers forming the graphene derivative and its aspect ratio[3] (e.g., largest lateral dimensions over minimum number of layers), yet the stabilization of single sheet graphene remains challenging and is often poorly compatible with common manufacturing processes, including solvent processing.[4–6] In contrast, graphene oxide (GO) is mass-producible and the oxygen moieties that dangle from the basal carbon plane enable aqueous suspensions of high-aspect ratio GO, with monolayer contents above 95%.

Regardless of the oxidation state of graphene, bulk properties of composites are strongly affected by the dispersion degree of the corresponding 2D platelets (e.g., interparticle distance vs processing methodology) in any matrix. Electrical conduction, for instance, requires sheet interconnectivity while mechanical load transfer is enhanced at higher dispersions.[7] Such concept has emerged as a rational tool[8] for tuning the conductive network of nanocomposites through the mesoscale distribution of their phases[9–11] mostly via physical procedures (e.g., segregation of polymer blends, shear/thermal-induced aggregation–diffusion or volume exclusion of conductive additives).

In this context, GO shows a dominant behavior that precludes interpreting composites through basic percolation theories. Concentrated GO dispersions are liquid crystals (LCs), displaying liquid-like fluidity and crystal-like mesomorphic order.[12] In such systems, LC nematic phases occur at concentrations low enough to obstruct association of GO into percolated networks.[13] Hence, reduced GO–polydimethylsiloxane (PDMS) fluids, where early orientation ordering occurs, leads to retarded percolation and exceptionally high dielectric permittivity materials.[14,15] Despite theoretical and experimental validation,[16–18] LC of nanocarbon/polymer composites diverges from previous reports where low percolation thresholds might have solely arisen from the physical gelation of graphenic additives within the matrix,[19] or due to their multilayer nature. This limitation calls for the design and further insight of reduced GO (rGO) composites displaying dynamic transitions between LC-like behavior and macroscopic percolated networks. The in-situ control of phase transitions in graphene assemblies, based on the regulation of molecular interactions rather than physical processing, has not been achieved previously.

Here we propose to regulate the transition between these two states via the introduction of photocleavable polymer brushes allowing the stabilization of GO prior to light-induced percolation. Therefore, the proposed approach is based on the regulation of supramolecular assembly, rather than physical control of phase transitions. We designed polymer brushes able to stabilize GO in apolar solvents and matrices and that can dissociate

Dr. M. Crespo, Dr. G. Santagiuliana, Dr. O. Picot, Dr. E. Bilotti, Dr. J. E. Gautrot
School of Engineering and Materials Science
Queen Mary University of London
Mile End Road, E1 4NS London, UK
E-mail: m.ribadeneyra@qmul.ac.uk; e.bilotti@qmul.ac.uk; j.gautrot@qmul.ac.uk
Dr. G. Santagiuliana, Dr. O. Picot, Dr. E. Bilotti
Nanoforce Technology Ltd.
Mile End Road, E1 4NS London, UK
Dr. G. Portale
Zernike Institute for Advanced Materials
University of Groningen
Nijenborgh 4, 9747 AG Groningen, The Netherlands
The ORCID identification number(s) for the author(s) of this article can be found under https://doi.org/10.1002/adfm.201900738.

DOI: 10.1002/adfm.201900738

upon photoirradiation. In particular, we demonstrate how the dynamic control of GO interfaces alters the phase distribution, interplatelet distance and the macroscopic electrical properties of rGO/PDMS composites.

2. Development of Photoresponsive Silicone-Based Polymer Brushes Stabilizing GO

Our polymer brushes consist of three domains (**Figure 1**a): 1) an amine-containing anchoring unit, promoting coupling to the surface of GO[20]; 2) a photocleavable *o*-nitrobenzyl derivative (NOB)[21] providing responsiveness; and 3) a PDMS chain providing compatibility with organic solvents and PDMS matrices (see the Methods section and Figures S1 to S12 in the Supporting Information). This NH_2–NOB–PDMS sequence enables the regulation of the dispersion the dispersion of associated GO/brush hybrids upon UV-light irradiation.

The NH_2–NOB–PDMS brush was dissolved in diethyl ether and gently stirred with a 1 mg mL^{-1} GO aqueous solution overnight, following Poulin et al.'s protocol,[14] leading to the extraction of the GO flakes into the organic phase (Figure 1b). Dispersions with concentrations between 0.5 and 5 wt% of GO in the PDMS liquid matrix (before curing) were birefringent, as observed with crossed polarizers (**Figure 2**c, bottom), indicating an LC order (Figure 1d), similar to that reported for other GO dispersions.[18] Anisotropic textures could also be observed by naked eye (Figure 1e; Figure S13, Supporting Information). Such behavior is attributed to the cofacial alignment of GO nanosheets within nematic domains with long-range order,[22] as to the total isotropic-to-nematic transition observed in GO solutions at concentrations above ≈0.5 wt%.[9] The observation of such an LC mesophase suggests that our GO/brush hybrids have a high degree of organization and alignment, indicating consistent and uniform interparticle distances arising from repulsive forces between adjacent hybrids.[23]

3. Impact of Photodestabilization on the Morphology and Rheological Properties of GO/Brush Hybrid Solutions

Upon UV exposure our hybrids are expected to cleave through the path illustrated in Figure 1f. When diluted dispersions were exposed to UV light, the initially stable solutions rapidly led to the precipitation of brown aggregates both in PDMS (Figure 1g, top) and in solvents (Figure 1h, inset). Similarly, the selective exposure of dispersions in PDMS (interposing a mask) caused the appearance of dark features in irradiated regions of the samples (Figure 1g). The UV–vis spectra (Figure 1h) confirmed the disappearance of the 310 nm absorption band of the NH_2–NOB–PDMS brush and the increase of the scattering contribution of GO upon photoirradiation. Photocleavage of the NOB moieties was also evidenced by FTIR (Figure 1i), with the appearance of bands at 1835–1797 cm^{-1} arising from the aromatic aldehyde formed.

Photodestabilization of the GO/brush hybrids was expected to affect their percolation as the polarized optical microscopy confirmed the significant decrease of birefringent features upon UV exposure (Figures 1j and 2k), which might be indicative of the disruption of LC phases, rich in GO/brush hybrids. We used photorheology to monitor changes in rheological profiles during UV irradiation (Figure 1e–g). Before UV, the GO/brush rigid domains result in a strong shear-thinning effect, with a pronounced hysteresis in the reverse shear sweep direction. After photodestabilization, both effects were considerably reduced.

Finally, frequency and strain sweeps further confirmed the change during photodestabilization (Figure 1f,g). In all samples, the loss modulus was predominant, confirming that materials are in a viscous sol state[24] and that association between GO platelets remains insufficient to enable the formation of a macroscopic network at this concentration. However, the evident drop in storage modulus upon photodestabilization indicates the reduction in physical association amongst adjacent LC GO/brush domains. In addition, samples prior to photodestabilization displayed a strong dependence of the storage modulus as a function of strain, with a strong shear thinning phenomenon, which could be attributed to slower relaxation times associated with low aspect ratio of LC domains, compared to high aspect ratio photodestabilized GO platelets.

4. Impact of the Photodestabilization of GO/Brush Hybrids on the Microstructure and Conductivity of Composites

Composites were cured using a Pt catalyst (see the Methods section in the Supporting Information). SEM analysis of the microstructure of cured and reduced composites containing up to a 10 wt% GO/brush hybrids (Figure 2a) revealed the formation of relatively stiff rGO-rich domains packed within the soft matrix. This is in agreement with the LC behavior observed prior curing, suggesting that the polymer-brush shell around GO platelets favors the formation of large and low aspect ratio LC-domains (17.6 ± 5.5 µm in length and 1.6 ± 0.6 µm in thickness). In these pockets, much thinner and smaller individual GO flakes with high aspect ratios (Figure 2b. *ca.* 1 µm long and 1.3 nm thick) are held together by brush side-chains, forming rGO/brush-rich regions within the PDMS matrix.

This lamellar-like structure, with two degrees of alignment (individual GO layers inside equivalently aligned rGO/brush-rich nematic domains), was confirmed by small-angle X-ray scattering (SAXS). Increasing the wt% of rGO/brush hybrid forces the platelets to enhance their alignment and minimize the excluded volume.[25] Accordingly, the diffraction peak q corresponding to the period between neighboring particles[26] shifts to higher values when increasing the concentration of GO from 0.5 to 5 wt% (Figure 2c). The evolution of d with the inverse of the volume fraction (ϕ) holds a linear relationship as: $d = t/\phi$, where t is the thickness of the diffracting elements forming the LC phase.[27,28] In our system, the linear dependence of d versus ϕ (Figure 2d,e) correlates with a thickness of ≈0.33 nm, close to the theoretical one for monolayer graphene (0.335 nm[29]), confirming the efficiency of the brush in maintaining the GO flakes individually isolated inside the larger rGO/brush-rich domains.

Despite thermal annealing at 200 °C, the conductivity of composites presented in Figure 2 remained very low, similar to that of the bare matrix (≈10^{-9} S m^{-1}), even at rGO loadings of 10 wt%. These samples had been prepared through the evaporation of

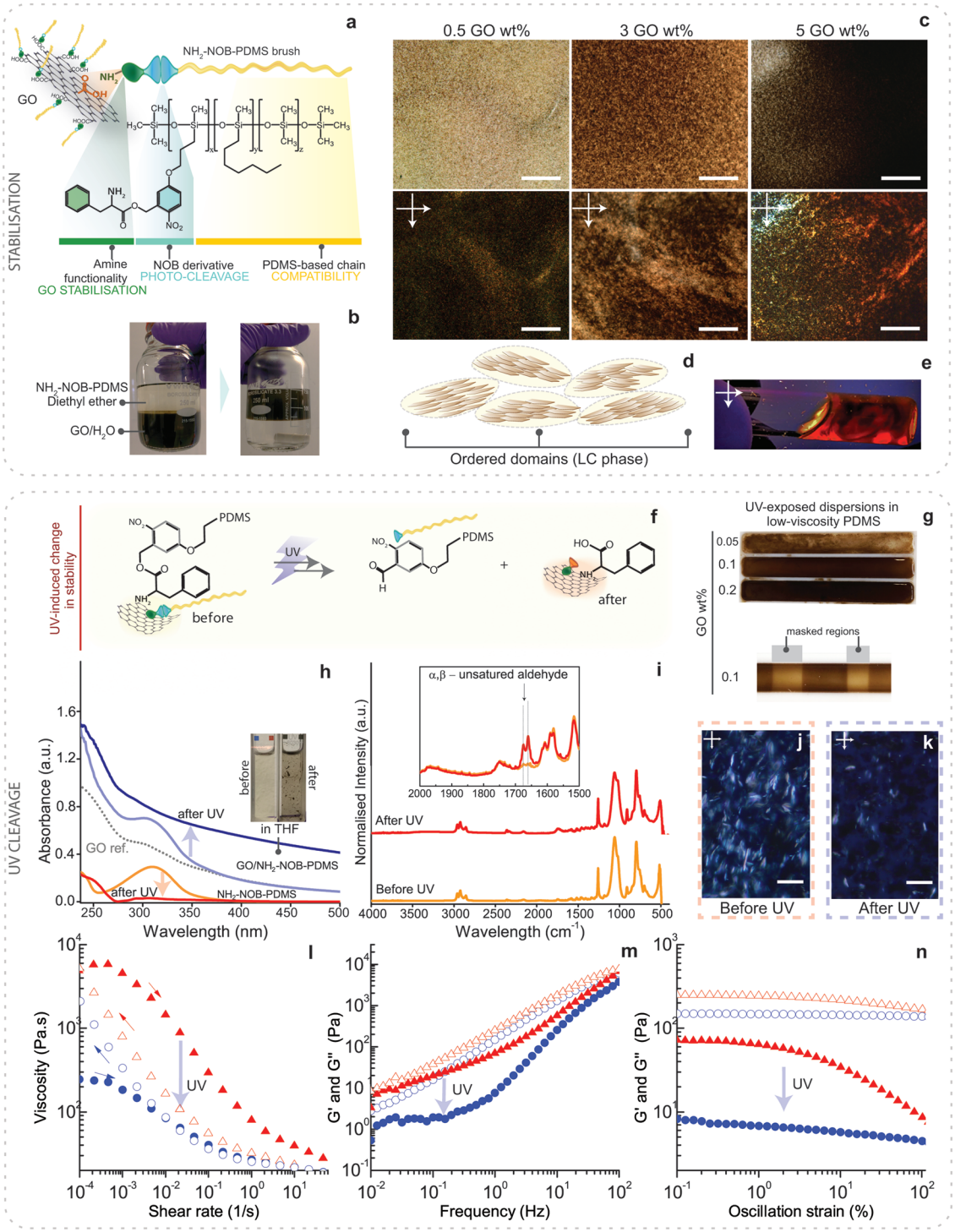

Figure 1. GO/brush hybrids: LC phase formation and photoresponsiveness. a) Schematic representation of the polymer brush structure stabilizing GO; b) phase transfer of GO into an organic phase (diethyl ether); c) optical microscopy images of varying GO/brush concentrations in the PDMS matrix without (top) and with crossed polarizers (bottom), scale bars are 200 µm; d) schematic representation of the liquid crystalline ordering (cofacial arrangement of GO platelets) and the formation of domains; e) optical image of a 0.5 wt% dispersion in THF between crossed polarizers; f) cleavage mechanism of the NH_2–NOB–PDMS/GO hybrids when exposed to UV light; g) images of PDMS (hydride terminated, $M_n \approx 580$ g mol^{-1}) dispersions containing 0.05, 0.5, and 1 wt% GO/brush concentrations after UV exposure and contrast between the darkened UV exposed areas and the nonexposed ones when a mask was interposed. h) FTIR spectra of the NH_2–NOB–PDMS brush before and after UV exposure; i) UV–vis spectra of the NH_2–NOB–PDMS/GO hybrids before and after UV exposure in THF (0.096 mg mL^{-1}); polarized optical microscopy (POM) images of the 1 wt% NOB–PDMS/GO PDMS preblends before j) and after k) exposure to UV light, scale bars are 20 µm; rheology characterization of 1 wt% GO preblends before (triangles, red) and after (circles, blue) exposure to UV light: l) shear sweeps, m) frequency sweeps, and n) strain sweeps. Closed symbols, G′; open symbols, G″.

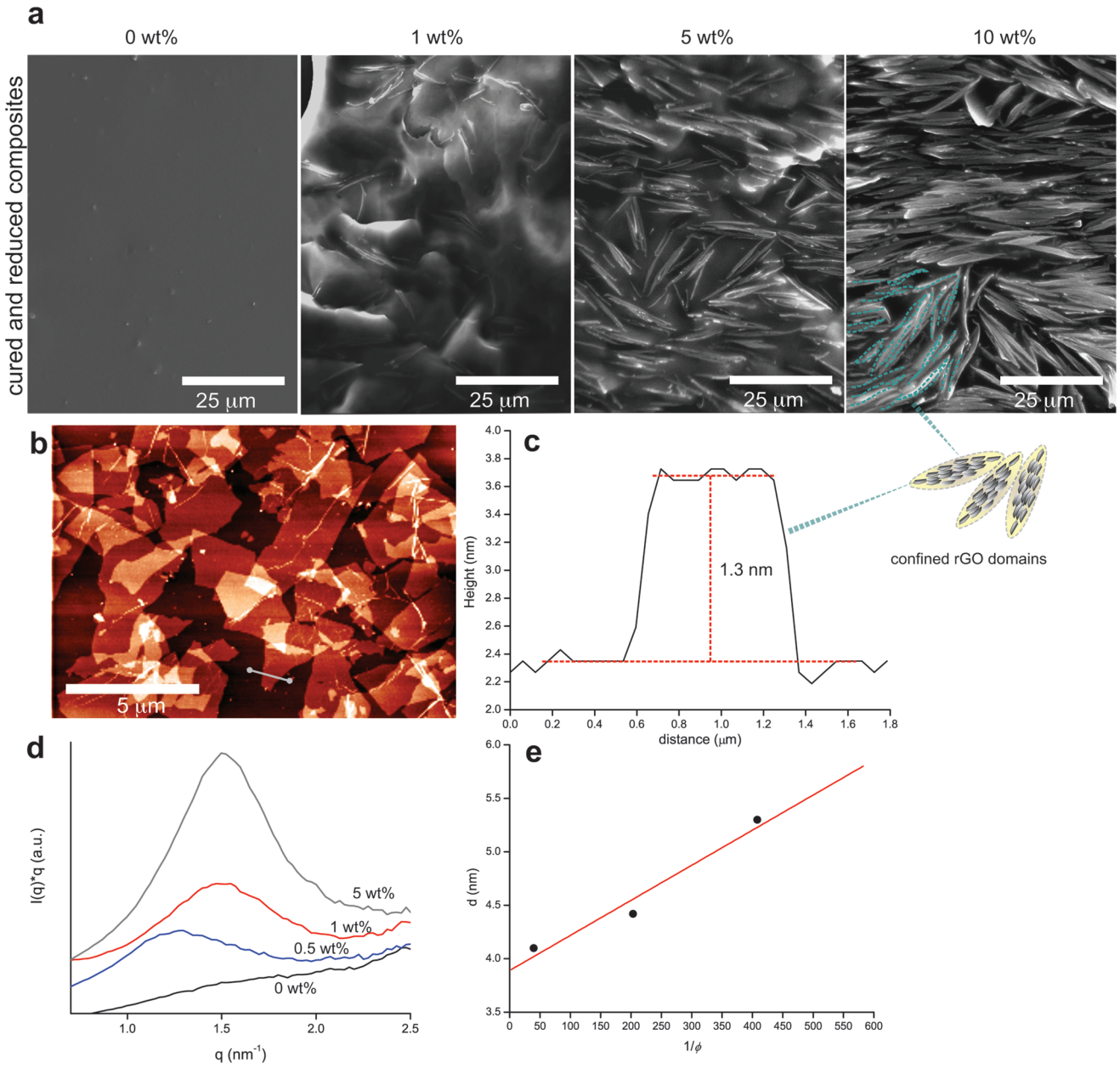

Figure 2. Footprint of the GO/brush LC phase in the microstructure of cured composites: a) SEM cross-sections of cured composites with varying rGO/brush concentrations in the PDMS matrix, after thermal reduction at 200 °C; b) AFM topography image of the pristine GO flakes deposited on a mica substrate; c) representative thickness profile of an individual GO flake with a thickness of 1.3 nm; and d) small-angle X-ray scattering patterns for cured and reduced composites showing the increase in signal intensity and decrease in interlayer distance when the concentration of GO increases; and e) linear relationship between the interlayer distance and volume fraction for these composites.

solvent from the matrix, followed by casting, photodestabilization and curing (Method A, **Figure 3**a). In contrast, when a concentrated THF solution of the hybrid (no matrix) was deposited onto a glass slide between two gold electrodes, evaporated, photodestabilized and annealed, the conductivity of the film increased significantly (Figure S14, Supporting Information). This indicates that the impeded electrical conduction observed in samples generated from processing method A arises from hindered percolation between LC domains in the matrix rather than insulation of rGO sheets by residual polymer brush coatings.

Since the partial reaggregation of colloids in the absence of shear is dependent on the viscosity of the dispersion,[30] we photodestabilized GO hybrids in dilute THF solutions, just prior to casting, curing and annealing (Method B, Figure 3a). Representative samples with 1 wt% GO/brush hybrids prepared through both methods display dramatically different microstructures (Figure 3b,c). At this GO concentration, samples prepared via method A display little connectivity between rGO-rich domains (Figure 3d). In contrast, samples prepared through method B displayed percolated and

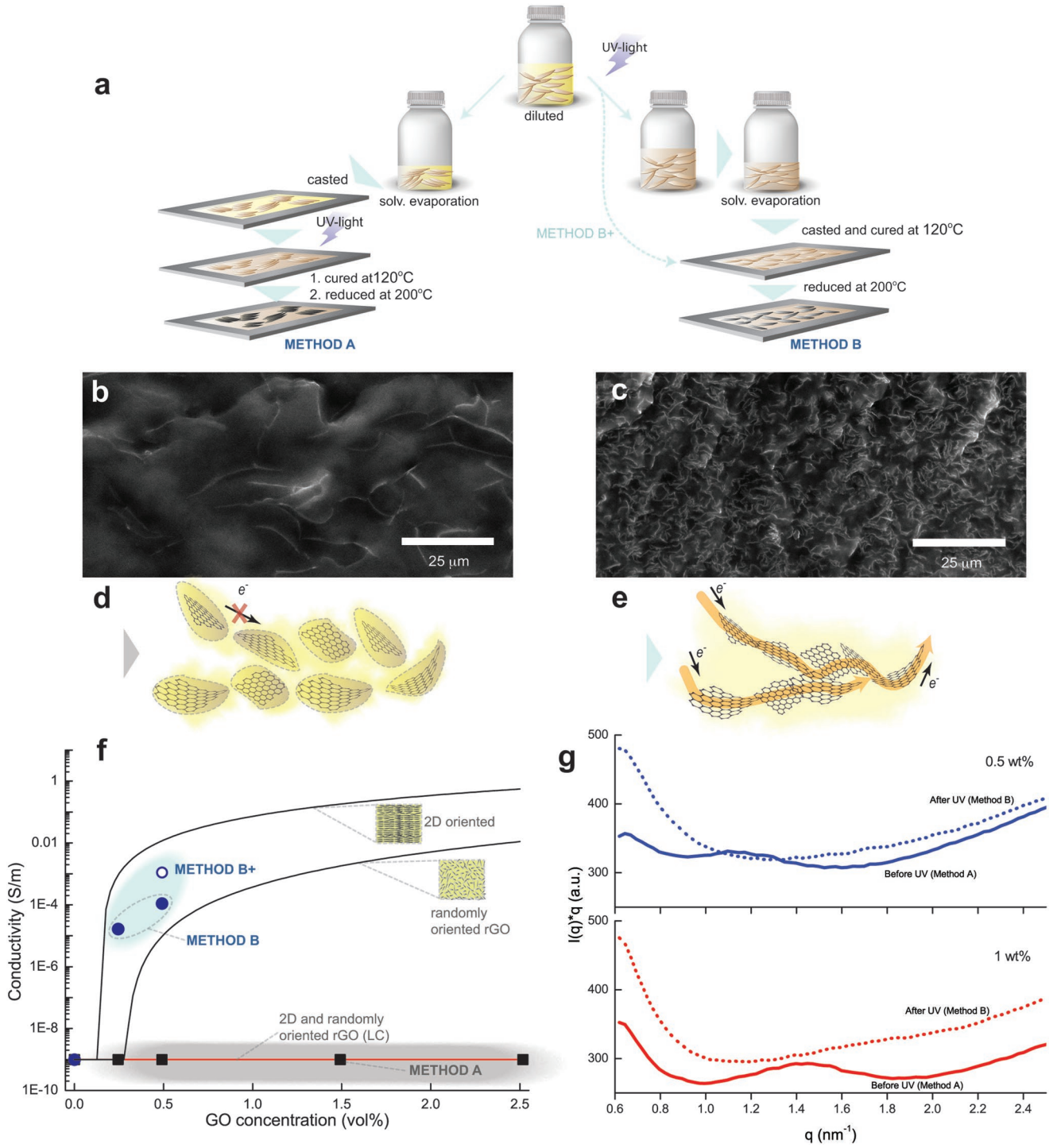

Figure 3. Kinetic entrapment of GO/brush reach domain and release upon UV exposure: a) schematic representation of the casting methods for the preparation of composites; SEM images of 1 wt% GO composite cross-sections prepared through Method A b) and Method B c); scheme showing how tunneling between rGO is hindered by their assembly into LC phases d) and restored upon exposure to UV light e); f) comparison of conductivities measured for rGO composites and composite theory predictions (non-LC and LC behavior, black and red solid lines, respectively); g) SAXS comparison showing how, for both concentrations (0.5 and 1 wt%), spatial order between rGO flakes is observed for samples prepared through Method A (before UV exposure) and then lost when these are diluted and irradiated (Method B).

randomly dispersed rGO-rich regions throughout the matrix, clearly forming a connected network (Figure 3e). Such observations suggest that, following photodestabilization, liquid crystalline phases are kinetically trapped in high viscosity matrices but can rearrange and allow percolation at low viscosities.[31]

In contrast to samples prepared through method A, samples from method B (photodestabilized when diluted) displayed expected conductivity levels (1.7×10^{-5} S m^{-1} for 0.5 wt% and 1.2×10^{-4} S m^{-1} for 1 wt% of rGO; Figure 3f). In addition, when photodestabilization was carried out on diluted samples, directly poured in the casting mold prior to solvent evaporation, curing and annealing (Method B+), the conductivity was further enhanced (to 1.1×10^{-3} S m^{-1}). This could potentially be attributed to the further reduction of viscosity of this sample when exposed to UV, or to the normal evaporation shearing, which could induce further platelet packing.[32]

We propose that the behavior of destabilized GO/brush composites is comparable to that observed in systems with antagonistic percolation: conductive and nonconductive particles compete to establish a network. Charge transfer efficiency decreases when the distance between conductive particles (d_c) increases; hence, if the nonconductive particles intercalate between the conductive ones above a critical volume fraction, d_c is enlarged beyond the maximum tunneling distance and electronic percolation is disabled.[31] In our system, the individual rGO flakes remain isolated due to the brush coverage and due to the formation of compact LC domains. By analogy then, both continuous networks of LC domains and brush are causing maximal rGO repulsion/isolation, preventing the formation of percolated rGO pathways. The system remains trapped in this configuration when films are photodestabilized at high viscosities (kinetically trapped state), but GO flakes quickly relax, reorganize and percolate when released from the brush shell in low viscosity media.

This analysis is supported by the clear loss of spatial order upon UV exposure for both 0.5 and 1 wt% GO samples. SAXS patterns show how the scattering peak arising from GO's cofacial packing, almost disappears in samples subjected to photodestabilization at low viscosity (Figure 3g). This confirms the destruction of the enveloping domains upon UV irradiation and the consequent decrease in cofacial alignment of rGO flakes and rGO/brush-rich domains once the stabilizing brush is photocleaved. Upon this loss, even slight orientational fluctuations might prompt percolation as a consequence of the lack of hindrance between neighboring platelets.

Classical models for a nanocomposite containing individual and well-distributed GO sheets (considering an aspect ratio ξ of ≈1000 and a density of 2 g cm^{-3} for GO[33]) estimates electrical percolation at 0.15 vol% (0.3 wt%), if the platelets are oriented in 2D, and at 0.28 vol% (0.57 wt%) when rGO is 3D randomly oriented (black lines in Figure 3f, see details in Section E in the Supporting Information). The experimental data obtained for our photodestabilized nanocomposites (prepared via methods B) fall in the region delimited by these predictions. In contrast, using the lower aspect ratio from the rGO/brush-rich LC domains (≈12.7, determined from SEM images), a percolation threshold of 9.5 vol% (*ca*. 18.2 wt%) is predicted (red line in Figure 3f). Therefore, we propose that photodestabilization regulates the phase transition of the LC GO/brush hybrids. We believe that the associated change in the aspect ratio of the rGO-rich features leads to a sharp transition to conductive composites (nearly two orders of magnitude higher).

5. Impact of Lamellar-Like Morphology on Matrix Reinforcement

In agreement with the conductivity data, increasing the rGO wt% in composites generated from Method A produced negligible mechanical reinforcement, independently from the UV treatment (**Figure 4**a–c). Such observations corroborate that in composites from Method A, the stiff LC domains (GO/brush-rich regions) have poor interfacial interactions. The reinforcement degree for these samples proved also significantly lower even than the prediction for 3D random GO orientation (solid black lines in Figure 4a, assuming individual and high aspect-ratio rGO flakes of elastic modulus of $E_f \approx 300$ GPa[34] in a PDMS matrix of $E_m = 0.21$ MPa; see further details in Supporting Information). Justified also by the rheological behavior, we propose that this phenomenon arises due to the entrapment of rGO inside the LC brush-rich domains. When the brush has not been released, the stiff and low aspect ratio domains do not interpenetrate and little mechanical reinforcement arises (Figure 4d).

To confirm this hypothesis, we iterated the general rule of mixtures using the dimensions and aspect ratio of the LC GO/brush-rich domains (solid red lines in Figure 4a) instead of those for individual GO layers. In addition to the aspect ratio and volume fraction of GO (V_{LC}), the orientation and length efficiency factors ($\eta_{o,LC}$ and $\eta_{L,LC}$, respectively) were also introduced in the model to account for the observed LC-behavior (see Section E in the Supporting Information). The experimental data obtained for non-photodestabilized nanocomposites (solid symbols, Figure 4a) fell within the region delimited by the predictions for 2D and 3D GO dispersion models, as our LC domains proved not well aligned but neither completely randomly oriented (seen in SEM images). Only at concentrations of GO below 0.5 vol% was the experimental reinforcement slightly outside of this region, presumably because such low concentrations the GO sheets cannot fully assemble as LC domains. In agreement with the percolation switch upon photodestabilization in diluted conditions (method B), mechanical reinforcement increased, falling within the region delimited by the predictions for the reinforcement of composites containing higher aspect-ratio GO sheets. This indicates that, releasing the rGO-brush linkage enables rGO sheets to establish interactions with the matrix and be able to confer mechanical reinforcement to a larger extent.

6. Origin of LC rGO/Brush-Rich Domains

Finally, to explore in more detail the nature of LC rGO/brush like domains, differential scanning calorimetry (DSC) was used. Profiles of the PDMS matrix formulation before and after incorporation of GO/brush hybrids (Figure 4e) show how the cold crystallization of PDMS almost disappears after mixing with GO/brush hybrids. The reduction of this transition implies the disorganization of crystallizable chains through interactions with the shell of GO/brush hybrids, possibly through surface confinement.[35,36] By analogy to the regimes observed in semidilute polymer solutions in bad-solvent conditions,[37] crystallizable PDMS chains from the matrix may contribute to the formation and confinement of the LC rGO/brush domains (Figure 4D), potentially due to their direct interaction with the polymer brush

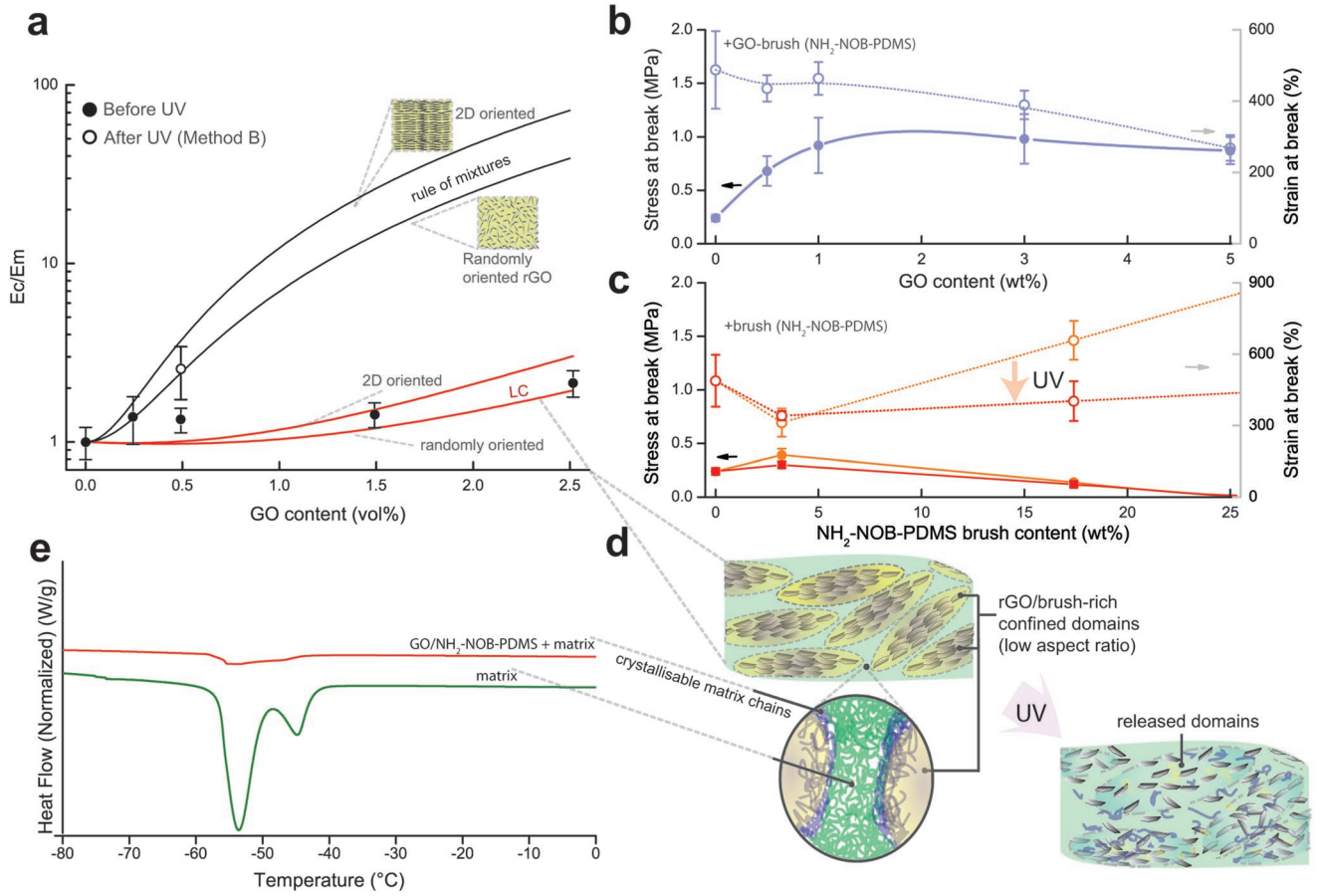

Figure 4. Origin of GO/brush domains formation and impact on mechanical reinforcement: a) reinforcement as a function of GO/brush concentration and associated theoretical predictions of the rule of mixtures for 3D randomly oriented and 2D-oriented GO platelets; b) mechanical characteristics of composites with varying GO/brush concentrations and c) analogous concentrations of brush in the matrix; d) schematic representation of the microstructure of mechanically under-reinforced composites displaying LC rGO/brush-rich domains (top), proposed molecular representation accounting for the interaction with the crystallizable matrix chains (bottom left) and released domains after UV irradiation and e) DSC thermograms showing the cold crystallization of the PDMS matrix with and without GO/brush hybrids.

shells. Such interaction with the crystallizable matrix chains would contribute to the formation of stiff LC domains, as we observed before UV exposure. Once these domains are diluted, the cleavage of the brush through UV unlocks this interaction and large LC domains do not develop. Once released, rGO sheets can interact with the matrix and between themselves, enabling percolation and mechanical reinforcement.

7. Conclusions

The ability to control the organization of graphene within matrices is a key challenge in the field of nanocomposites. Light addressable systems, such as the one developed in this study, demonstrate the feasibility of controlling the architecture of such nanomaterials while retaining excellent processing characteristics, through the regulation of phase transitions in the sol state. Our observations confirm the complexity of graphene architectures in solutions and the impact that such graphene/graphene interactions may have on the processing and performance of associated nanocomposites. It emerges that the kinetic trapping of intermediate states is an attractive route to control the morphology and organization of percolated graphene networks. Considering the wide range of polymer-brush chemistries that have been developed in other contexts, this approach should be applicable to most polymeric matrices relevant to the development of nanocomposites. Other stimuli-responsive strategies could also achieve similar control of sol state behaviors and help addressing some of the processing challenges that have hindered the wider application of graphene derivatives. Therefore, this study calls for a more systematic investigation of molecular parameters regulating the responsive and phase transition behavior of graphenic nanomaterials and solutions, and their integration to processing methodologies for the fabrication of a wide range of nanocomposites for structural and energy applications.

Supporting Information

Supporting Information is available from the Wiley Online Library or from the author.

Acknowledgements

Results reported in this piece of research are part of a project that has received funding from the European Union's Horizon 2020 research and innovation programme under the Marie Skłodowska-Curie grant agreement SILGRAFUN No 703020 and Innovate UK (EPSRC, EP/M507726/1).

Conflict of Interest

The authors declare no conflict of interest.

Keywords

graphene, liquid crystal, nanocomposite, photoresponsive, polymer brush

Received: January 22, 2019
Revised: March 8, 2019
Published online: April 14, 2019

[1] V. Singh, D. Joung, L. Zhai, S. Das, S. I. Khondaker, S. Seal, *Prog. Mater. Sci.* **2011**, *56*, 1178.
[2] R. J. Young, I. A. Kinloch, L. Gong, K. S. Novoselov, *Compos. Sci. Technol.* **2012**, *72*, 1459.
[3] Y. Li, H. Zhang, M. Crespo, H. Porwal, O. Picot, G. Santagiuliana, Z. Huang, E. Barbieri, N. M. Pugno, T. Peijs, E. Bilotti, *ACS Appl. Mater. Interfaces* **2016**, *8*, 24112.
[4] L. Gong, I. A. Kinloch, R. J. Young, I. Riaz, R. Jalil, K. S. Novoselov, *Adv. Mater.* **2010**, *22*, 2694.
[5] Y. Zhu, S. Murali, W. Cai, X. Li, J. W. Suk, J. R. Potts, R. S. Ruoff, *Adv. Mater.* **2010**, *22*, 3906.
[6] H. J. Salavagione, G. Martínez, G. Ellis, *Macromol. Rapid Commun.* **2011**, *32*, 1771.
[7] G. Santagiuliana, O. T. Picot, M. Crespo, H. Porwal, H. Zhang, Y. Li, L. Rubini, S. Colonna, A. Fina, E. Barbieri, A. B. Spoelstra, G. Mirabello, J. P. Patterson, L. Botto, N. M. Pugno, T. Peijs, E. Bilotti, *ACS Nano* **2018**, *12*, 9040.
[8] H. Deng, L. Lin, M. Ji, S. Zhang, M. Yang, Q. Fu, *Prog. Polym. Sci.* **2014**, *39*, 627.
[9] W. Bauhofer, S. C. Schulz, A. E. Eken, T. Skipa, D. Lellinger, I. Alig, E. J. Tozzi, D. J. Klingenberg, *Polymer* **2010**, *51*, 5024.
[10] I. Alig, P. Pötschke, D. Lellinger, T. Skipa, S. Pegel, G. R. Kasaliwal, T. Villmow, *Polymer* **2012**, *53*, 4.
[11] M. Badard, A. Combessis, A. Allais, L. Flandin, *Mater. Chem. Phys.* **2017**, *191*, 89.
[12] J. E. Kim, T. H. Han, S. H. Lee, J. Y. Kim, C. W. Ahn, J. M. Yun, S. O. Kim, *Angew. Chem., Int. Ed.* **2011**, *50*, 3043.
[13] M. Mathew, T. Schilling, M. Oettel, *Phys. Rev. E* **2012**, *85*, 061407.
[14] J. Yuan, A. Luna, W. Neri, C. Zakri, T. Schilling, A. Colin, P. Poulin, *Nat. Commun.* **2015**, *6*, 8700.
[15] J. Yuan, A. Luna, W. Neri, C. Zakri, A. Colin, P. Poulin, *ACS Nano* **2018**, *12*, 1688.
[16] R. Basu, D. Kinnamon, A. Garvey, *Appl. Phys. Lett.* **2015**, *106*, 201909.
[17] M. Kumar, A. Gowda, S. Kumar, *Part. Part. Syst. Charact.* **2017**, *34*, 1700003.
[18] S. Kale, F. A. Sabet, I. Jasiuk, M. Ostoja-Starzewski, *J. Appl. Phys.* **2016**, *120*, 045105.
[19] A. R. Koltonow, C. Luo, J. Luo, J. Huang, *ACS Omega* **2017**, *2*, 8005.
[20] S. Pandit, M. De, *J. Phys. Chem. C* **2017**, *121*, 600.
[21] J. C. Grim, I. A. Marozas, K. S. Anseth, *J. Controlled Release* **2015**, *219*, 95.
[22] C. Zakri, C. Blanc, E. Grelet, C. Zamora-Ledezma, N. Puech, E. Anglaret, P. Poulin, *Philos. Trans. R. Soc., A* **2013**, *371*, 20120499.
[23] Z. Xu, C. Gao, *Nat. Commun.* **2011**, *2*, 571.
[24] K. D. Q. Nguyen, W. V. Megone, D. Kong, J. E. Gautrot, *Polym. Chem.* **2016**, *7*, 5281.
[25] C. Zamora-Ledezma, N. Puech, C. Zakri, E. Grelet, S. E. Moulton, G. G. Wallace, S. Gambhir, C. Blanc, E. Anglaret, P. Poulin, *J. Phys. Chem. Lett.* **2012**, *3*, 2425.
[26] F. Tardani, W. Neri, C. Zakri, H. Kellay, A. Colin, P. Poulin, *Langmuir* **2018**, *34*, 2996.
[27] N. Puech, C. Blanc, E. Grelet, C. Zamora-Ledezma, M. Maugey, C. Zakri, E. Anglaret, P. Poulin, *J. Phys. Chem. C* **2011**, *115*, 3272.
[28] P. Poulin, R. Jalili, W. Neri, F. Nallet, T. Divoux, A. Colin, S. H. Aboutalebi, G. Wallace, C. Zakri, *Proc. Natl. Acad. Sci. USA* **2016**, *113*, 11088.
[29] Z. H. Ni, H. M. Wang, J. Kasim, H. M. Fan, T. Yu, Y. H. Wu, Y. P. Feng, Z. X. Shen, *Nano Lett.* **2007**, *7*, 2758.
[30] D. Chen, M. Doi, *J. Colloid Interface Sci.* **1999**, *212*, 286.
[31] A. V. Kyrylyuk, M. C. Hermant, T. Schilling, B. Klumperman, C. E. Koning, P. Van Der Schoot, *Nat. Nanotechnol.* **2011**, *6*, 364.
[32] Y. Xia, T. S. Mathis, M.-Q. Zhao, B. Anasori, A. Dang, Z. Zhou, H. Cho, Y. Gogotsi, S. Yang, *Nature* **2018**, *557*, 409.
[33] D. G. Papageorgiou, I. A. Kinloch, R. J. Young, *Prog. Mater. Sci.* **2017**, *90*, 75.
[34] C. Gómez-Navarro, M. Burghard, K. Kern, *Nano Lett.* **2008**, *8*, 2045.
[35] A. B. Shivanandareddy, M. Kumar, V. Lakshminarayanan, S. Kumar, *RSC Adv.* **2015**, *5*, 47692.
[36] S. Lu, S. Li, J. Yu, Z. Yuan, B. Qi, *RSC Adv.* **2013**, *3*, 8915.
[37] F. Monroy, L. R. Arriaga, D. Langevin, *Phys. Chem. Chem. Phys.* **2012**, *14*, 14450.